IRis

Northeastern University

Physics Faculty Publications

Department of Physics

August 15, 1981

effective-medium theory of electronic states in structurally disordered metals: Application to liquid Cu

L. Huisman
Brandeis University

D. Nicholson
Brandeis University

L. Schwartz
Brandeis University

A. Bansil
Northeastern University

Recommended Citation

Huisman, L.; Nicholson, D.; Schwartz, L.; and Bansil, A., "effective-medium theory of electronic states in structurally disordered metals: Application to liquid Cu" (1981). *Physics Faculty Publications.* Paper 368.

This work is available open access, hosted by Northeastern University.

PHYSICAL REVIEW B VOLUME 24, NUMBER 4 15 AUGUST 1981

Effective-medium theory of electronic states in structurally disordered metals: Application to liquid Cu

L. Huisman, D. Nicholson, and L. Schwartz
Department of Physics, Brandeis University, Waltham, Massachusetts 02254

A. Bansil
Department of Physics, Northeastern University, Boston, Massachusetts 02115
(Received 20 March 1980; revised manuscript received 16 March 1981)

We consider the application of the effective-medium approximation (EMA) to the muffin-tin model of a liquid metal. The spherical symmetry of the average liquid is used to reduce the momentum ($\vec{k}$)-dependent self-consistency requirements of the theory to a form in which they involve one-dimensional rather than three-dimensional integrations. We also show that, within the EMA, a closed expression for the integrated density of states can be derived, and that this expression provides a useful check on the convergence of the self-consistent equations. The theory is applied to liquid Cu. The self-consistent equations converge without difficulty and the resulting electronic spectrum is in substantial agreement with recent photoemission data. Our results are compared with an alternate approach to the muffin-tin EMA suggested by Asano and Yonezawa. The two approaches yield similar densities of states but markedly different behavior for the special functions.

I. INTRODUCTION

In random substitutional alloys it is well established that the coherent-potential approximation (CPA) provides a satisfactory mean-field theory of the electronic structure of strong scattering systems.[1,2] Of the various extensions of the CPA to the liquid-metal problem,[3–5] it is generally agreed that the most promising is Roth's effective-medium approximation (EMA). While the EMA has been studied in detail in connection with the tight-binding model,[6] only limited results are available regarding its application to the more realistic muffin-tin model.[7–9]

The general features of the muffin-tin EMA are summarized in Sec. II A. In this connection it is instructive to compare various features of the CPA and EMA. In the alloy problem, the quantity to be determined self-consistently is the CPA effective scattering matrix $\tau_L(E)\delta_{LL'}$ (here L and L' are angular momentum indices). By contrast, in the case of structural disorder the EMA is formulated in terms of the effective atomic scattering matrix $T_l(E)\delta_{LL'}$ and the effective structure functions $\tilde{B}_{LL'}(\vec{k},E)$. Thus the EMA self-consistency conditions involve quantities that are explicitly momentum dependent and are intrinsically more difficult to satisfy. We show in Sec. II A, however, that the EMA integral equations can be reduced to scalar (i.e., one-dimensional) form by expressing the results of all angular integrations in terms of easily tabulated functions of the angular indices.[10]

In Sec. II B we consider alternate methods for computing the average electronic spectrum. Here it turns out that the CPA and EMA have one important feature in common: both lead to closed expressions for the integrated density of states $N(E)$.[7,11] The EMA result for $N(E)$ is derived Appendix C and is employed in Sec. III to check the degree to which the EMA self-consistency conditions have been satisfied. To conclude the discussion in Sec. II B, the results of our calculations (which are an exact treatment of the muffin-tin EMA) are compared with those obtained by combining the atomic-sphere approximation with the EMA.[9] The latter approach is found to give densities of states that are in good agreement with our results. However, we show that one cannot interpret the atomic-sphere spectral densities as the conventional momentum decomposition of the average spectrum

 ©1981 The American Physical Society

and, therefore, it is not surprising that the atomic-sphere results differ *qualitatively* from the spectral densities obtained in the present calculations.

In Sec. III we consider the application of the EMA to liquid Cu. Our calculations include the effects of s, p, and d phase shifts[12] and are based on experimentally determined atomic densities and radial distribution functions.[13] The self-consistent equations derived in Sec. II A were found to converge without difficulty and the resulting spectrum is in good agreement with the results of photoemission measurements on molten Cu.[14] (A more detailed comparison of muffin-tin EMA calculations on liquid Cu and other liquid d-band metals with the available experimental data will be presented in a forthcoming paper.)

It should be noted that our present findings are considerably more positive than those presented in connection with our earlier work on the s-resonance model.[7] It now appears that the difficulties regarding the analytic properties of the EMA encountered in Ref. 7 were to a large extent due to the unphysical character of the model.[15] It is clear that further numerical and analytic work will have to be done to establish the range within which the EMA may be reliably applied to the muffin-tin Hamiltonian.

II. MUFFIN-TIN EMA

A. General equations

In the muffin-tin model of a liquid metal the electrons are scattered by a disordered array of nonoverlapping spherical potentials.[7–9] In a specific configuration of the system, suppose that N ions, located at the points $\vec{R}_1, \vec{R}_2, \ldots, \vec{R}_N$ are distributed within a volume Ω. The total one-electron potential $\mathcal{V}(\vec{r})$ at the point $\vec{r}$ is then a sum of contributions, $v_\alpha(\vec{r}) \equiv v(|\vec{r}-\vec{R}_\alpha|)$, each of which is centered at one of the atomic sites. Since it is assumed that the individual potentials do not overlap, $\mathcal{V}(\vec{r})$ is nonvanishing with a sphere of radius r_m (the muffin-tin radius) surrounding each of the atomic centers and may be taken equal to zero in the region between the spheres.

In multiple-scattering theory the electronic states of the system are described in terms of the configuration and energy-dependent total scattering operator $\mathcal{T} = \mathcal{V}(1 - G_0\mathcal{V})^{-1}$. [Here $G_0 = (E^+ - H_0)^{-1}$ is the free-electron propagator and $E^+ \equiv E + i0^+$.] The quantity of physical interest, however, is $\langle \mathcal{T} \rangle$ where the angular brackets indicate an average over all possible configurations of the atomic scattering centers. In the framework provided by the muffin-tin model, the formal analysis of the multiple-scattering series proceeds most directly in the angular momentum representation. Within the EMA, the plane-wave matrix element $\langle \vec{k} | \langle \mathcal{T} \rangle | \vec{k} \rangle$ may be calculated as[17]

$$\langle \vec{k} | \langle \mathcal{T} \rangle | \vec{k} \rangle = (4\pi)^2 n \sum_{LL'} i^{(l'-l)} Y_L^*(\vec{k}) \times Q_{LL'}(k,\vec{k}) Y_{L'}(\vec{k}) \ , \quad (2.1)$$

where

$$Q_{LL'}(k,\vec{k}') = T_l(k,k')\delta_{LL'} + [T_l(k,\kappa)/T_l] T_{LL'}(\vec{k}') \times [T_{l'}(\kappa,k')/T_{l'}] \ , \quad (2.2a)$$

$$T_l(k,k') = t_l(k,k') + t_l(k,\kappa) f_l(\kappa) t_l(\kappa,k') \ , \quad (2.2b)$$

$$T_{LL'}(\vec{k}) = T_l \{ \tilde{B}(\vec{k})[1 - T\tilde{B}(\vec{k})]^{-1} \}_{LL'} T_{l'} \ , \quad (2.2c)$$

$E = \kappa^2$, and $T_l \equiv T_l(\kappa,\kappa)$. Here $L \equiv (l,m)$ is a composite angular index, $Y_L(\vec{x})$ is the usual spherical harmonic of the angles of $\vec{x}$, $n \equiv N/\Omega$ is the mean atomic density, and the quantities $t_l(k,k')$ are the angular components of the $\vec{k} - \vec{k}'$ matrix element of the atomic scattering operator corresponding to the individual muffin-tin potential $v(r)$.[16,18] Equations (2.1) and (2.2) express $\langle \vec{k} | \langle \mathcal{T} \rangle | \vec{k} \rangle$ in terms of two of two basic objects: $\tilde{B}_{LL'}(\vec{k})$ and $f_l(\kappa)$. These are defined by the following pair of coupled nonlinear equations (see Appendix A):

$$\tilde{B}_{LL'}(\vec{k}) = B_{LL'}(\vec{k}) + \sum_{L_1} \frac{1}{n} \int \frac{d^3k_1}{(2\pi)^3} h(|\vec{k} - \vec{k}_1|) T_l^{-1} T_{LL_1}(\vec{k}_1) \tilde{B}_{L_1L'}(\vec{k}_1) \quad (2.3a)$$

and

$$f_l(\kappa) = \sum_{L_1} \frac{1}{n} \int \frac{d^3k_1}{(2\pi)^3} B_{LL_1}(\vec{k}_1) \{ T_{L_1L}(\vec{k}_1) - T_{l_1}[\tilde{B}_{L_1L}(\vec{k}_1) - B_{L_1L}(\vec{k}_1)] T_l \} \tau_l^{-1} - \sum_{L_1} \frac{n}{\tau_l} \int d\vec{R}_\beta g(0|\beta) h(0|\beta) B_{LL_1}(0|\beta) T_{l_1} B_{L_1L}(\beta|0) T_l \ . \quad (2.3b)$$

Here $h(k)$ is the Fourier transform of $h(\alpha|\beta) \equiv g(\alpha|\beta) - 1$, $g(\alpha|\beta) \equiv g(|\vec{R}_\alpha - \vec{R}_\beta|)$ is the radial distribution function, $\tau_l(E) \equiv t_l(\kappa,\kappa)$, and the matrices $B(0|\beta)$ and $B(\vec{k})$ are defined by the relations

$$B_{LL'}(\vec{k}) = n \int d\vec{R}_\beta g(0|\beta) e^{i\vec{k}\cdot\vec{R}_\beta} B_{LL'}(0|\beta) \tag{2.4a}$$

$$= \sum_{L_1} B_{l_1}^{ll'}(k) C_{L'L_1}^{L} Y_{L_1}^*(\vec{k}) \ , \tag{2.4b}$$

where[16]

$$B_{l_1}^{ll'}(k) = (4\pi)^2 n i^{(l-l')} \left[\frac{(k/\kappa)^{l_1}}{E - k^2} - i\kappa \int_0^\infty R^2 dR\, j_{l_1}(kR) h_{l_1}(\kappa R) h(R) \right] \ , \tag{2.5}$$

$$C_{L'L_1}^{L} = \int d\Omega_{\vec{x}} Y_L^*(\vec{x}) Y_{L'}(\vec{x}) Y_{L_1}(\vec{x}) \tag{2.6}$$

and $h_l(x)$ denotes the outgoing spherical Hankel function.

Equations (2.3) are the central equations of the muffin-tin EMA. Their solution, as noted above, is a substantial undertaking because, for each energy a pair of coupled nonlinear integral equations must be solved for $T_l(E)$ and $\tilde{B}_{LL'}(\vec{k})$ in terms of the basic input units $t_l(k,k')$, n, and $g(R)$. This aspect of the EMA can not be avoided without introducing further approximations. In addition, Eqs. (2.3) are complicated by the vector character of the various $\vec{k}$-space integrations. It is this second point to which we now address our attention. We will show that, by introducing somewhat larger matrices, the EMA equations can be written in a form that requires integration over just the scalar variable $k \equiv |\vec{k}|$.[10]

The essential point in the reduction is to note that the isotropic character of the average liquid implies that the $\vec{k}$ dependence of the renormalized matrices $\tilde{B}_{LL'}(\vec{k})$ and $T_{LL'}(\vec{k})$ is no more complicated than that of the simpler object $B_{LL'}(\vec{k})$. Recalling Eq. (2.4b) we write

$$\tilde{B}_{LL'}(\vec{k}) = \sum_{L_1} \tilde{B}_{l_1}^{ll'}(k) C_{L'L_1}^{L} Y_{L_1}^*(\vec{k}) \ , \tag{2.7a}$$

and

$$T_{LL'}(\vec{k}) = \sum_{L_1} T_{l_1}^{ll'}(k) C_{L'L_1}^{L} Y_{L_1}^*(\vec{k}) \ . \tag{2.7b}$$

Substituting into Eq. (2.3b) we have

$$f_l(\kappa) = \sum_{L_1 L_2 L''} (n\tau_l)^{-1} \int \frac{d^3k}{(2\pi)^3} B_{l_1}^{ll''}(k) \{ T_{l_2}^{l''l}(k) - T_{l''}[\tilde{B}_{l_2}^{l''l}(k) - B_{l_2}^{l''l}(k)] T_l \} C_{L''L_1}^{L} C_{LL_2}^{L''} Y_{L_1}^*(\vec{k}) Y_{L_2}^*(\vec{k})$$

$$- \sum_{L_1 L_2 L''} n\tau_l^{-1} \int d\vec{R}\, g(R) h(R) B_{l_1}^{ll''}(R) T_{l''} B_{l_2}^{l''l}(R) T_l C_{L''L_1}^{L} C_{LL_2}^{L''} Y_{L_1}^*(\vec{R}) Y_{L_2}^*(\vec{R}) \ , \tag{2.8}$$

where $B_{l_1}^{ll'}(R) = -4\pi\kappa i^{(l-l')} h_{l_1}(\kappa R)$. Using the identities

$$\sum_{m_2} C_{LL_2}^{L''} Y_{L_2}^*(\vec{x}) = \sum_{m_2} C_L^{L''L_2} Y_{L_2}(\vec{x}) \tag{2.9a}$$

and

$$\sum_{m''m_1} C_{L''L_1}^{L} C_{L'}^{L''L_1} = \delta_{LL'} g(l\,|\,l''\,|\,l_1)/(2l+1) \tag{2.9b}$$

where

$$C_L^{L''L_1} = \int Y_{L''}^*(\vec{x}) Y_{L_1}^*(\vec{x}) Y_L(\vec{x}) d\Omega_{\vec{x}} \ , \tag{2.9c}$$

$$g(l\,|\,l''\,|\,l_1) = \frac{(2l+1)(2l_1+1)(2l''+1)}{8\pi} \int_{-1}^{1} P_l(x) P_{l_1}(x) P_{l''}(x) dx \ , \tag{2.9d}$$

and $P_l(x)$ is a Legendre polynomial, the scalar form of Eq. (2.8) is

$$f_l(\kappa)=\tau_l^{-1}\sum_{l''l_1}\frac{g(l\,|\,l''\,|\,l_1)}{(2l+1)}\left[\frac{1}{n}\int_0^\infty\frac{dk\,k^2}{(2\pi)^3}B_{l_1}^{ll''}(k)\{T_{l_1}^{l''l}(k)-T_{l''}[\tilde{B}_{l_1}^{l''l}(k)-B_{l_1}^{l''l}(k)]T_l\}\right.$$
$$\left.-n\int_0^\infty R^2dr\,g(R)h(R)B_{l_1}^{ll''}(R)T_{l''}B_{l_1}^{l''l}T_l\right]\ . \tag{2.10}$$

Consider next the equation relating $T(\vec{k})$ to $\tilde{B}(\vec{k})$ and T. Combining Eqs. (2.2c), (2.7), and (2.9b) we find

$$T_{l_1}^{ll'}(k)=T_l\tilde{B}_{l_1}^{ll'}(k)T_{l'}+\sum_{l''l_2l_3}T_l\tilde{B}_{l_2}^{ll''}(k)T_{l_3}^{l''l'}(k)\begin{bmatrix}l_1 & l_2 & l_3\\ l'' & l' & l\end{bmatrix}[g(l\,|\,l'\,|\,l_1)]^{-1}\ , \tag{2.11}$$

where the six-l symbols are defined as[19]

$$\begin{bmatrix}l_1 & l_2 & l_3\\ l'' & l' & l\end{bmatrix}=\sum_{mm'm''m_1m_2m_3}C_{L_1}^{L_2L_3}C_L^{L'L_1}C_{L''L_2}^{L}C_{L'L_3}^{L''}\ . \tag{2.12}$$

Similarly, Eq. (2.3a) reduces to

$$\tilde{B}_{l_1}^{ll'}(k)=B_{l_1}^{ll'}(k)+\sum_{l''l_2l_3}\frac{2}{n\pi}\int_0^\infty k_1^2dk_1h_{l_1}(k,k_1)T_l^{-1}T_{l_2}^{ll''}(k_1)\tilde{B}_{l_3}^{l''l'}(k_1)\begin{bmatrix}l_1 & l_2 & l_3\\ l'' & l' & l\end{bmatrix}[g(l\,|\,l'\,|\,l_1)]^{-1}\ , \tag{2.13}$$

where

$$h_l(k,k_1)=n\int R^2dR\,j_l(kR)h(R)j_l(k_1R)\ . \tag{2.14}$$

The summations in Eqs. (2.11) and (2.13) can be understood in terms of conventional matrix operations. For example, introducing the *superindices* $\lambda=l\otimes l_1$, and $\lambda''=l''\otimes l_3$ and defining

$$T_{l_1}^{ll'}(k)\equiv T_\lambda^{l'}(k),\quad T_{l_3}^{l''l'}(k)\equiv T_{\lambda''}^{l'}(k)\ ,$$
$$T_l\tilde{B}_{l_1}^{ll'}(k)\equiv\gamma_\lambda^{l'}(k)\ , \tag{2.15a}$$

and

$$\sum_{l_2}T_l\tilde{B}_{l_2}^{ll''}(k)\begin{bmatrix}l_1 & l_2 & l_3\\ l'' & l' & l\end{bmatrix}[g(l\,|\,l'\,|\,l_1)]^{-1}\equiv D_{\lambda\lambda''}^{l'}(k)\ , \tag{2.15b}$$

Eq. (2.11) can formally be inverted as

$$T_\lambda^{l'}(k)=\sum_{\lambda''}\{[1-D(k)]^{-1}\}_{\lambda\lambda''}\gamma_{\lambda''}^{l'}(k)T_{l'} \tag{2.16}$$

Similarly, Eq. (2.13) can be rewritten as

$$\tilde{B}_\lambda^{l'}(k)=B_\lambda^{l'}(k)+\sum_{\lambda''}\frac{2}{n\pi}\int_0^\infty k_1^2dk_1d_{\lambda\lambda''}^{l'}(k,k_1)\tilde{B}_{\lambda''}^{l'}(k_1)\ , \tag{2.17}$$

where $\tilde{B}_{l_1}^{ll'}(k)\equiv\tilde{B}_\lambda^{l'}(k)$, $B_{l_1}^{ll'}(k)\equiv B_\lambda^{l'}(k)$, and

$$\sum_{l_2}h_{l_1}(k,k_1)T_l^{-1}T_{l_2}^{ll''}(k)\begin{bmatrix}l_1 & l_2 & l_3\\ l'' & l' & l\end{bmatrix}[g(l\,|\,l'\,|\,l'')]^{-1}\equiv d_{\lambda\lambda''}^{l'}(k,k_1)\ . \tag{2.18}$$

B. The average spectrum

Once T_l and $B_{LL'}$ are available, there remains the problem of evaluating the average density of electronic states, $\rho(E)$. In principle, $\rho(E)$ is to be calculated from the relation

$$\pi\rho(E)=-\mathrm{Im}\,\mathrm{Tr}[\langle\mathcal{G}(E^+)\rangle]\ , \tag{2.19}$$

where $\langle\mathcal{G}\rangle=G_0+G_0\langle\mathcal{T}\rangle G_0$. Without introducing any additional approximations, Eq. (2.19) can be implemented by three equivalent methods. First, by integrating the spectral density $A(\vec{k},E)$ (Ref. 17):

$$\rho(E)=\frac{2}{n}\int A(\vec{k},E)\frac{d^3k}{(2\pi)^3} \tag{2.20a}$$

where

$$A(\vec{k},E)=\frac{2(4\pi)^2 n}{N\,|E^+-k^2|^2}\sum_{LL'L_1L_1'} Y_L(\vec{k})Q^*_{L_1L}(\kappa,\vec{k})S_{L_1L_1'}(\vec{k})Q_{L_1'L'}(\kappa,\vec{k})Y^*_{L'}(\vec{k}) \tag{2.20b}$$

and

$$S_{LL'}(\vec{k})=(2i)^{-1}\{[T^{-1}-(T^{-1})^*]\delta_{LL'}-[\tilde{B}(\vec{k})-\tilde{B}^\dagger(\vec{k})]_{LL'}\}. \tag{2.20c}$$

Second, by using the Lloyd equation[8,20]

$$\rho(E)=\frac{\sqrt{E}}{2\pi^2 n}-\frac{2}{\pi}\,\mathrm{Im\,Tr}\left[T\frac{d\tau^{-1}}{dE}-n\int d^3R_\alpha\;T(0\,|\,\alpha)\frac{d}{dE}B(\alpha\,|\,0)\right] \tag{2.21}$$

where

$$T(\alpha\,|\,0)=n^{-1}\int e^{-i\vec{k}\cdot\vec{R}_\alpha}\;T(\vec{k})\frac{d^3k}{(2\pi)^3}\;, \tag{2.22}$$

and $B(\alpha\,|\,0)$ is defined by Eqs. (2.4), and third, by differentiating the following expression for $N(E)$ (see Appendix C):

$$N(E)=\frac{E^{3/2}}{3\pi^2 n}+\frac{2}{\pi}\,\mathrm{Im\,Tr}\left[\ln(T)-\frac{1}{n}\int\frac{d^3k}{(2\pi)^3}\ln[1-T\tilde{B}(\vec{k})]\right.$$
$$\left.+\frac{n}{2}\int d^3R_\alpha\;g(0\,|\,\alpha)h(0\,|\,\alpha)T\hat{B}(0\,|\,\alpha)T\hat{B}(\alpha\,|\,0)\right] \tag{2.23}$$

where

$$\hat{B}(\alpha\,|\,0)=B(\alpha\,|\,0)+n^{-1}\int\frac{d^3k}{(2\pi)^3}\tilde{B}(\vec{k})T\tilde{B}(\vec{k})[1-T\tilde{B}(\vec{k})]^{-1}e^{-i\vec{k}\cdot\vec{R}_\alpha}\;. \tag{2.24}$$

[In Eqs. (2.21) and (2.23) the Tr and ln operations refer to implicit angular indices.]

In connection with Eqs. (2.20), two points should be noted. First, we show in Appendix B that solutions of the EMA equations (2.3) occur in conjugate pairs. At each energy E, these two solutions give opposite signs for $A(\vec{k},E)$ [i.e., $A(\vec{k},E)\to -A(\vec{k},E)$] and, therefore, opposite signs for $\rho(E)$. [While a physically acceptable solution must have $A(\vec{k},E)>0$ for all $\vec{k}$, there is at present no proof that either solution will have this property.[15,21]] Second, it is evident from Eqs. (2.2) and (2.20) that the structure of $A(\vec{k},E)$ will be dominated by the roots of the secular equation

$$||T^{-1}-\tilde{B}(\vec{k})||=0\;. \tag{2.25}$$

Since the liquid is, after averaging, an isotropic system, we need only consider vectors $\vec{k}$ along the z axis. For these $\vec{k}$ the matrix $\tilde{B}_{LL'}(k)$ is diagonal in m and m' [i.e., $\tilde{B}_{LL'}(\vec{k})\to\tilde{B}^m_{l,l'}(k)\delta_{m,m'}$] and the complex bands defined by (2.25) can be classified as $m=0$, $m=1$, $m=2,\ldots,$ etc. However, once $\vec{k}$ is oriented along the z axis, the factors $Y^*_L(\vec{k})$ and $Y_{L'}(\vec{k})$ on the right side of (2.20b) give rise to $\delta_{m,0}$ and $\delta_{m',0}$, respectively, and it can easily be shown that *only the $m=0$ complex bands contribute to $A(k,E)$.* Similar behavior is found in the non-self-consistent quasicrystalline approximation (QCA) (Ref. 22) and would appear to be characteristic of all mean-field theories of structurally disordered systems.

In connection with Eq. (2.23) we emphasize that the derivation outlined in Appendix C makes repeated use of the fact that T and $\tilde{B}(\vec{k})$ satisfy the EMA equations. Accordingly, (2.23) will yield results equivalent to those obtained via (2.20) and (2.21) only if the self-consistency requirements of the theory have been satisfied. Thus Eq. (2.23), in addition to providing an alternate method for calculating $\rho(E)$, allows us to monitor the sensitivity of the electronic spectrum to the degree of self-consistency attained in the solution of the EMA equations (2.3).

Finally, we comment on another approach to the muffin-tin EMA proposed by Asano and Yonezawa.[9] These authors obtain $\tilde{B}_{LL'}(\vec{k})$ and T_l by solving equations equivalent to (2.3) but, rather

than using the exact relations (2.20) and (2.21), calculate $A(\vec{k},E)$ and $\rho(E)$ by employing what they refer to as an atomic-sphere approximation. This approach is based on the relation

$$\rho(\vec{r}+\vec{R},\vec{r}'+\vec{R}') \equiv \frac{-1}{\pi}\,\mathrm{Im}\langle \vec{r}+\vec{R}\,|\,G_{\vec{R},\vec{R}'}\,|\,\vec{r}'+\vec{R}\rangle$$
$$= \frac{-E}{\pi}\,\mathrm{Im}\sum_{LL'} Y_L(\vec{r})R_l(r)[T_l\delta(\vec{R}-\vec{R}')\delta_{LL'} + nT_{LL'}(\vec{R}\,|\,\vec{R}')]R_{l'}(r')Y^*_{L'}(\vec{r}') \ . \quad (2.26)$$

Here $G_{\vec{R},\vec{R}'}$ denotes the restricted average of the one-electron Green's function in which the ions centered at $\vec{R}$ and $\vec{R}'$ are assumed to be fixed ($\vec{R}$ and $\vec{R}'$ may be equal), $T(\vec{R}\,|\,\vec{R}')$ is defined by Eqs. (2.22), and $R_l(r)$ denotes the radial atomic wave function normalized to

$$R_l = j_l(\kappa r)\cot(\delta_l) - n_l(\kappa r) \quad (2.27)$$

for $r \geq r_m$. It should be understood that Eq. (2.26) is valid only if $\vec{r}$ and $\vec{r}'$ are confined to the muffin-tin spheres centered at $\vec{R}$ and $\vec{R}'$, respectively. For example, in the case $\vec{R}=\vec{R}'$ we have the following expression for the local charge density within the muffin-tin sphere surrounding an atom whose position is held fixed at the origin

$$\rho(E\,|\,r) = \frac{-E}{\pi}\,\mathrm{Im}\sum_{L} Y_L(\vec{r})R_l(r)T_lR_l(r)Y^*_L(\vec{r}) \ . \quad (2.28)$$

In the atomic-sphere approximation (2.27) is used to extend (2.28) for $r > r_m$ and the density of states is then calculated as

$$\rho(E) = 4\pi\int_0^{r_{\mathrm{WS}}} dr\, r^2\rho(E\,|\,r) \ , \quad (2.29)$$

where $r_{\mathrm{WS}} = (3/4\pi n)^{1/3}$ is the radius of the effective Wigner-Seitz sphere.

In Fig. 1 we compare the results of a calculation based on the atomic-sphere approximation with those of a calculation based on the exact equations (2.19). (Both calculations employ a simplified model of liquid Cu in which the atomic potentials are represented by just a single resonant $l=2$ phase shift.[23]) The close agreement between these two results reflects the fact that most of the d-charge density is localized within the muffin-tin sphere and is correctly represented by Eq. (2.29). Using related arguments, Asano and Yonezawa suggest the following expression for the spectral function:

$$A(\vec{k},E) = \frac{-E}{\pi}\,\mathrm{Im}\sum_{LL'}\left[\int_0^{r_{\mathrm{WS}}} R_l^2(r)r^2dr\right]^{1/2}[T_l\delta_{LL'} + T_{LL'}(\vec{k})]\left[\int_0^{r_{\mathrm{WS}}} R_{l'}^2(r)r^2dr\right]^{1/2} . \quad (2.30)$$

We note, however, that the right-hand side of (2.30) does not vanish for large k [since $T_{LL'}(\vec{k})\to 0$ as $k\to\infty$] and, therefore, that $\rho(E)$ cannot be calculated by the usual identity (2.20a). In fact, the relation between Eqs. (2.30) and (2.29) is

$$\rho(E) = \lim_{k\to\infty} A(\vec{k},E) \ . \quad (2.31)$$

In addition, we note that part of the structure in the atomic-sphere spectral densities is related to the free-electron singularities of $\tilde{B}(\vec{k})$. By contrast, when Eq. (2.20b) is used to compute $A(\vec{k},E)$, the factor $|E^+ - k^2|^{-2}$ compensates for the singularity in $\tilde{B}(\vec{k})$ and all of the structure in the resulting spectral functions is directly related to the determinant $||T^{-1} - \tilde{B}(\vec{k})||$ [recall Eq. (2.25)]. This point is illustrated in Fig. 2 where the EMA and atomic-sphere spectral functions are compared (at $E=0.5$ Ry) for the $l=2$ Cu resonance model. The unphysical minimum at $k\approx 0.7$ in the atomic-sphere case is due entirely to free-electron singularities in $\tilde{B}(\vec{k})$.[24]

III. RESULTS FOR LIQUID Cu

In this section we present the results of muffin-tin EMA calculations for liquid Cu. The pair distribution function and atomic density were taken from experimental data on molten Cu at 1150 °C.[13] Standard techniques were used to evaluate the ionic potentials[12] and, as usual, scattering effects corresponding to $l \geq 3$ have been neglected. Our EMA calculations are based on Eqs. (2.20). At $E=0.3$ and 0.5 Ry our results were checked by using Eq.

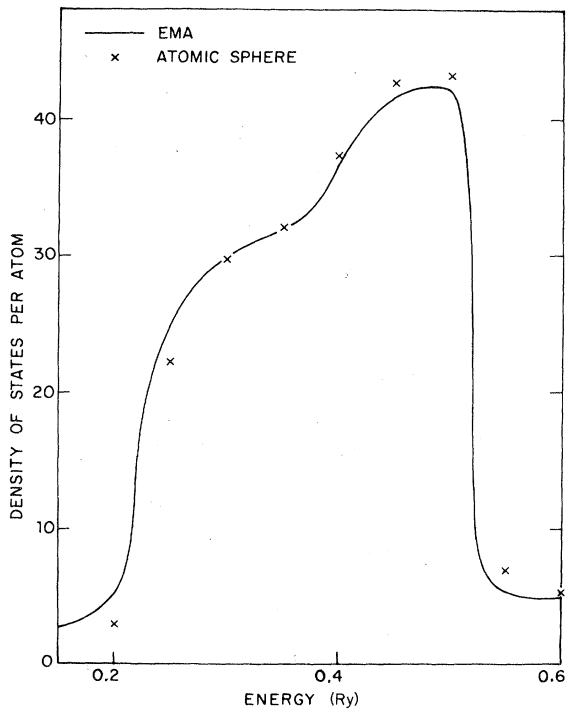

FIG. 1. EMA (solid) and atomic-sphere (crosses) densities of states (electrons per atom per Ry) for Cu d-resonance model.

(2.23) to compute $N(E)$ at neighboring energies and then evaluating $\rho(E)$ by numerical differentiation. These two methods agreed to within one percent at both energies. This level of agreement may be taken as a measure of the degree of self-consistency attained in the solution of the original EMA equations.

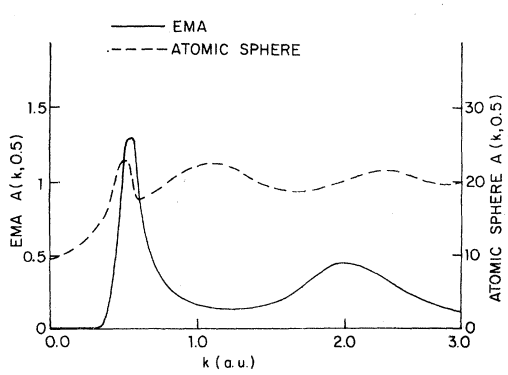

FIG. 2. EMA (solid) and atomic-sphere (dashed) spectral density functions for Cu d-resonance model at $E = 0.5$ Ry. Note that the vertical scales differ significantly.

In Fig. 3(a) we see that the EMA density of states is in substantial agreement with the photoemission data on molten Cu at 1087 °C.[14,25] [We show both the photoemitted energy distribution curve (EDC) and the derived optical density of states (ODS).] In Fig. 3(b), the EDC for an annealed Cu crystal[14] (727 °C) is compared with the calculated density of states for crystalline Cu.[26] The three curves in Fig. 3(a) all show an asymmetric d-band peak with a width of roughly 0.35 Ry and a well-defined upper edge.[25] It should be noted that the present comparison suffers from the usual limitations due to matrix element, correlation, and other effects neglected in the theory. In particular the differences between the theoretical and experimental curves in the low-energy region of Fig. 3(a) (i.e., between 0.2 and 0.4 Ry) are probably due, in large part, to the aforementioned shortcomings since similar differences are also seen in Fig. 3(b).

The EMA density of states shown in Fig. 3(a) is quite similar to that obtained in the $l = 2$ calculation shown in Fig. 1 above. This agreement is not surprising since the s and p phase shifts are weak and slowly varying throughout the resonance region. The increased structure in Fig. 3(a) near $E = 0.25$ Ry is due to enhanced s-d coupling at low energies. It should be emphasized that (in both cases) the EMA results are in sharp contrast with the QCA density of states which has an unphysically narrow d band and with the MQCA spectrum which becomes negative in the resonance region.[27]

Spectral functions computed via Eq. (2.20b) are shown in Fig. 4. We find sharp quasiparticle peaks in the weak- scattering regime and a more diffuse structure characteristic of localized states in the resonance region. In particular, while outside the resonance region practically all the weight is in the sharp peaks, inside the d band a sizable contribution to the density of states comes from the high-k part of $A(k,E)$.

ACKNOWLEDGMENTS

This work was supported in part by the National Science Foundation Grant No. DMR-80-23440 (L.H., D.N., and L.S.) and Grant No. DMR-79-02600 (A.B.).

APPENDIX A

In this appendix our aim is to clarify the structure of Eq. (2.3b). Combining the definition (2.2b) with the operator version of the EMA equations,[5,8] the most natural expression for $f_l(\kappa)$ is

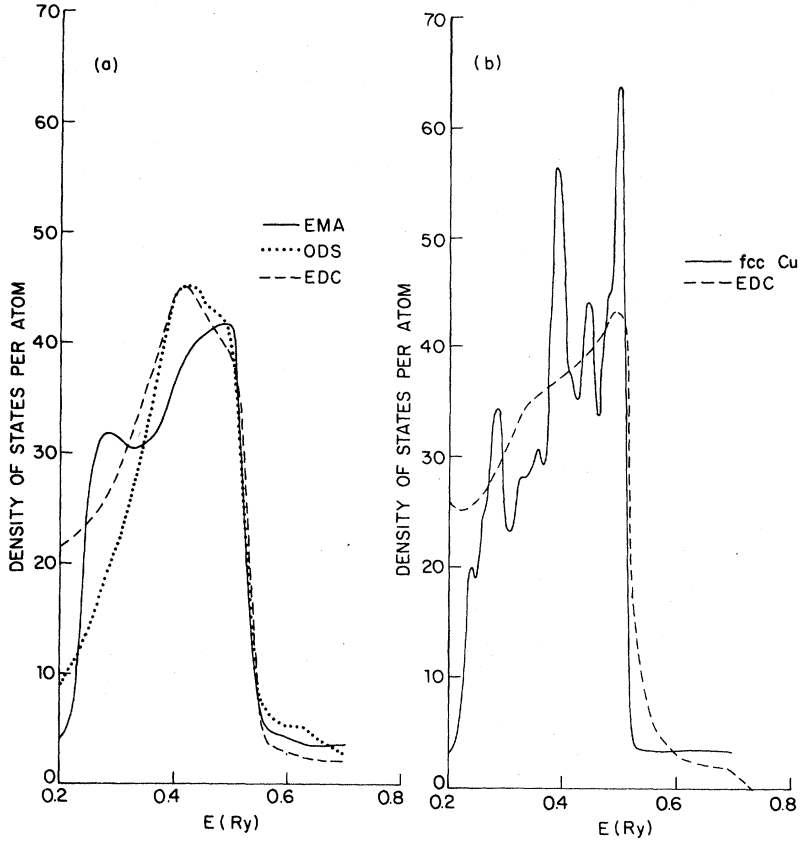

FIG. 3. (a) Calculated EMA density of states is compared with the experimental EDC and ODS for molten Cu. (b) Calculated crystal Cu density of states is compared with the experimental EDC.

$$f_l(\kappa) = \sum_{L_1} \frac{1}{n} \int \frac{d\vec{k}}{(2\pi)^3} b_{LL_1}(\vec{k}) T_{L_1 L}(\vec{k}) \tau_l^{-1} \tag{A1}$$

with

$$b_{LL_1}(\vec{k}) = \sum_{L_2} \frac{(4\pi)^2 n}{E - k^2} i^{l-l_1} \left[\frac{k}{\kappa}\right]^{l_2} C^L_{L_1 L_2} Y^*_{L_2}(\vec{k}) \ ,$$

and where $C^L_{L_1 L_2}$ is defined in Eq. (2.6). Note that (A1) is meaningful only when l_2 is not larger than 3, i.e., when l and l_1 are not larger than 1, because otherwise the integrand diverges. This divergence is caused by the singular behavior of $B_{LL'}(0\,|\,\beta)$ at $\beta = 0$. In order to avoid this divergence, the equations have to be written such that $B_{LL'}(0\,|\,\beta)$ is always multiplied by $g(0\,|\,\beta)$. This leads to the more complicated expression for $f_l(\kappa)$ given in Eq. (2.3b).

APPENDIX B

In this appendix it will be shown that solutions to the EMA equations come in pairs. First, $B_{LL'}(0\,|\,\beta)$ [Eq. (2.4a)] can be written as

$$B_{LL'}(0\,|\,\beta) = B^{(1)}_{LL'}(0\,|\,\beta) + B^{(2)}_{LL'}(0\,|\,\beta) \ , \tag{B1a}$$

$$B^{(1)}_{LL'}(0\,|\,\beta) = 4\pi\kappa \sum_{L_1} i^{l-l'+l_1} C^L_{L'L_1} Y_{L_1}(\vec{R}_\beta) n_{l_1}(\kappa R_\beta), \tag{B1b}$$

$$B^{(2)}_{LL'}(0\,|\,\beta) = -4\pi i\kappa \sum_{L_1} i^{l-l'+l_1} C^L_{L'L_1} Y_{L_1}(\vec{R}_\beta) j_{L_1}(\kappa R_\beta) \ . \tag{B1c}$$

Second, we note that

$$[B^{(1)}_{LL'}(0\,|\,\beta)]^* = B^{(1)}_{L'L}(\beta\,|\,0) \tag{B2}$$

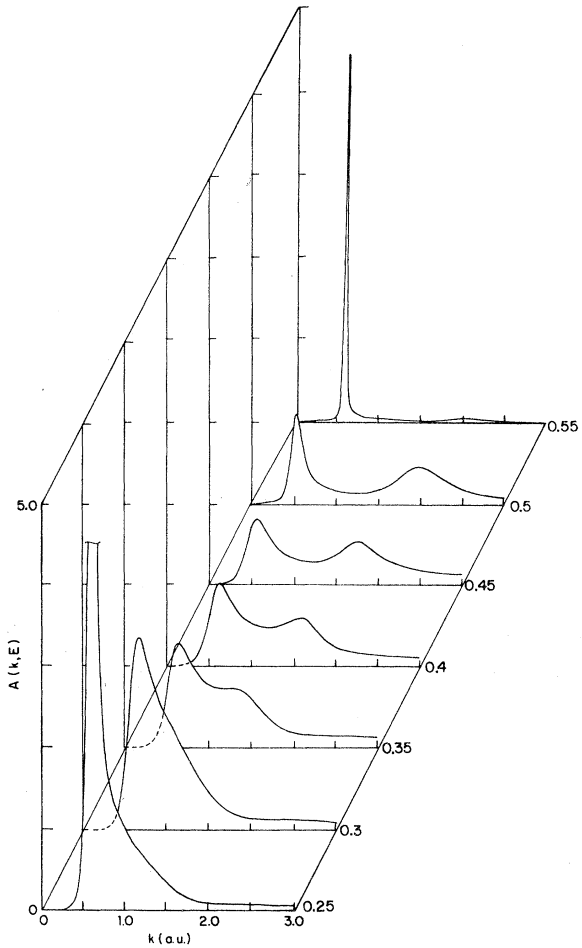

FIG. 4. EMA spectral densities as a function of k for energies between $E = 0.25$ and 0.55 Ry.

and introduce the auxiliary quantity

$$\widetilde{B}^{(2)}_{LL'}(\alpha\,|\,\beta) = \widetilde{B}_{LL'}(\alpha\,|\,\beta) - B^{(2)}_{LL'}(\alpha\,|\,\beta) \quad , \tag{B3}$$

where

$$\widetilde{B}_{LL'}(\alpha\,|\,\beta) = \frac{1}{n}\int \frac{d^3k}{(2\pi)^3} e^{-i\vec{k}\cdot(\vec{R}_\alpha - \vec{R}_\beta)} \widetilde{B}_{LL'}(\vec{k}) \quad , \tag{B4}$$

in terms of T_l and $\widetilde{B}^{(2)}_{LL'}(\alpha\,|\,\beta)$. The EMA equations (2.3) can be written as

$$T_{LL'}(\alpha\,|\,\beta) = T_l \widetilde{B}^{(2)}_{LL'}(\alpha\,|\,\beta) T_{l'} + T_l \sum_{L_1} n \int \widetilde{B}^{(2)}_{LL_1}(\alpha\,|\,\gamma) T_{L_1L'}(\alpha\,|\,\beta) d\vec{R}_\gamma \, , \tag{B5a}$$

$$T_l^{-1} = (\tau_l^{-1} - i\kappa) - \sum_{L_1} n \int B^{(1)}_{LL_1}(0\,|\,\beta) T_{L_1L}(\beta\,|\,0) d\vec{R}_\beta T_l^{-1} \, , \tag{B5b}$$

and

$$\widetilde{B}^{(2)}_{LL'}(\alpha\,|\,\beta) = n^{-1} g(\alpha\,|\,\beta) B^{(1)}_{LL'}(\alpha\,|\,\beta) + n^{-1} h(\alpha\,|\,\beta) T_l^{-1} \times \sum_{L_1} n \int T_{LL_1}(\alpha\,|\,\gamma) \widetilde{B}^{(2)}_{L_1L'}(\gamma\,|\,\beta) d\vec{R}_\gamma \, . \tag{B5c}$$

In Eqs. (B5), $(\tau_l^{-1} - i\kappa)$, $g(\alpha\,|\,\beta)$, and $h(\alpha\,|\,\beta)$ are real. It follows from (B2) that if the matrices $\widetilde{B}^{(2)}(\alpha\,|\,\beta)$ and T are solutions of (B5), then $[\widetilde{B}^{(2)}(\alpha\,|\,\beta)]^\dagger$ and $T^\dagger$ are also solutions. Fourier-transforming, it can easily be shown that the same statement holds for $\{\widetilde{B}^{(2)}(\vec{k}), T\}$ and $\{[\widetilde{B}^{(2)}(\vec{k})]^\dagger, T^\dagger\}$.

To show that the two solutions of the EMA equations correspond to opposite signs for $A(k,E)$ we note that $B^{(2)}_{LL'}(\vec{k})$ is proportional to $\delta(E - k^2)$. Because of the external factor $|E - k^2|^{-2}$ in (2.20b), such singular terms do not influence $A(\vec{k},E)$ and the only effect of going from one solution to the other is a sign change in the matrix $S(\vec{k})$.

APPENDIX C

We begin the derivation of Eq. (2.23) by observing that $\widehat{B}(\alpha\,|\,\beta)$ [defined by (2.24)] satisfies the following identities:

$$T(\alpha\,|\,\beta) = g(\alpha\,|\,\beta) T \widehat{B}(\alpha\,|\,\beta) T \tag{C1a}$$

and

$$\widetilde{B}(\alpha\,|\,\beta) = B(\alpha\,|\,\beta) + h(\alpha\,|\,\beta)\widehat{B}(\alpha\,|\,\beta) \quad . \tag{C1b}$$

Returning to the Lloyd equation (2.21), we observe that the last two terms on the right-hand side can be rewritten as

$$\begin{aligned} -\mathrm{Tr}\left[T\frac{d\tau^{-1}}{dE}\right] = -\mathrm{Tr}\left[T\frac{dT^{-1}}{dE}\right] + \mathrm{Tr}\frac{1}{n}\int \frac{d^3k}{(2\pi)^3}T\frac{d\widetilde{B}(\vec{k})}{dE} \\ - \mathrm{Tr}\, n \int d\vec{R}_\alpha \Bigg[T(0\,|\,\alpha)\frac{d}{dE}[B(\alpha\,|\,0) - \widetilde{B}(\alpha\,|\,0)] \\ - T[B(0\,|\,\alpha) - \widetilde{B}(0\,|\,\alpha)]\frac{d}{dE}[T(\alpha\,|\,0)T^{-1}]\Bigg] \end{aligned} \tag{C2a}$$

and

$$\begin{aligned} \mathrm{Tr}\, n \int d\vec{R}_\alpha T(0\,|\,\alpha)\frac{d}{dE}B(\alpha\,|\,0) = \mathrm{Tr}\frac{1}{n}\int \frac{d^3k}{(2\pi)^3}T(\vec{k})\frac{d}{dE}\widetilde{B}(\vec{k}) \\ + \mathrm{Tr}\, n \int d\vec{R}_\alpha T(0\,|\,\alpha)\frac{d}{dE}[B(\alpha\,|\,0) - \widetilde{B}(\alpha\,|\,0)] \quad . \end{aligned} \tag{C2b}$$

Note that both (C1) and (C2) are valid only if T and $\widetilde{B}(\vec{k})$ satisfy the EMA self-consistency requirements (2.3). Adding Eqs. (C2), we find

$$\begin{aligned} \Delta\rho(E) = \frac{2}{\pi}\,\mathrm{Im}\frac{d}{dE}\mathrm{Tr}\ln(T) - \frac{2}{\pi n}\,\mathrm{Im}\frac{d}{dE}\,\mathrm{Tr}\int \frac{d^3k}{(2\pi)^3}\ln[1 - T\widetilde{B}(\vec{k})] \\ + \frac{2n}{\pi}\,\mathrm{Im}\,\mathrm{Tr}\int d\vec{R}_\alpha T[B(0\,|\,\alpha) - \widetilde{B}(0\,|\,\alpha)]\frac{d}{dE}[T(\alpha\,|\,0)T^{-1}] \quad . \end{aligned} \tag{C3}$$

In deriving (C3) we have used the fact that $T(\alpha\,|\,\beta)\to 0$ as $|\vec{R}_\alpha - \vec{R}_\beta| \to 0$ [cf. (C1a) by adding to the right-hand side]

$$0 = \frac{2}{n\pi}\,\mathrm{Im}\,\mathrm{Tr}\int \frac{d^3k}{(2\pi)^3}\widetilde{B}(\vec{k})[1 - T\widetilde{B}(\vec{k})]^{-1}\frac{dT}{dE} \quad . \tag{C4}$$

Using the identities (C1) to rewrite the last term in (C3) we immediately obtain the result $\rho(E) = d[N(E)]/dE$, where $N(E)$ is given by (2.23).

---

[1]G. M. Stocks, W. M. Temmerman, and B. L. Gyorffy, Phys. Rev. Lett. 41, 339 (1978).

[2]A. Bansil, Phys. Rev. Lett. 41, 1670 (1978); Phys. Rev. B 20, 4025 (1979); 20, 4035 (1979).

[3]B. L. Gyorffy, Phys. Rev. B 1, 3290 (1970); J. Korringa and R. L. Mills, *ibid.* 5, 1654 (1972).

[4]L. Schwartz and H. Ehrenreich, Ann. Phys. (N.Y.) 64, 100 (1971).

[5]L. M. Roth, Phys. Rev. B 9, 2476 (1974).

[6]L. M. Roth, J. Phys. F 6, 2267 (1976).

[7]L. Huisman, L. Schwartz, and A. Bansil, J. Phys. (Paris) 41, C8-441 (1980).

[8]V. A. Singh and L. Roth, Phys. Rev. B 21, 4403 (1980).

[9]S. Asano and F. Yonezawa, J. Phys. F 10, 75 (1980).

[10]An alternate approach to this reduction is discussed in Ref. 9.

[11]In the case of the EMA this result has been discussed by Niiseki [(J. Phys. F 9, L185 (1979)] within the framework of the tight-binding model. In the alloy problem see Refs. 1 and 2.

[12]The construction of the underlying atomic potential is described in A. Bansil, H. Ehrenreich, L. Schwartz, and R. E. Watson, Phys. Rev. B 9, 445 (1974), Appendix C.

[13]Y. Waseda and M. Ohtani, Phys. Status Solidi B 62, 535 (1974).

[14]G. P. Williams and C. Norris, J. Phys. F 4, L175 (1974); C. Norris, Inst. Phys. Conf. Proc. 30, 171 (1977).

[15]In Ref. 7 we demonstrated by explicit numerical calculation that the EMA can lead to *negative* spectral functions. This finding is consistent with our earlier formal

work [L. Schwartz, Phys. Rev. B 21, 522 (1980)] and renders futile any attempt to prove that the EMA and CPA are on the same analytic footing. In addition, we found that convergence of the self-consistent equations could be quite problematic in the s-resonance model. In Ref. 8, Singh and Roth considered an $l = 0$ resonance that was centered at higher energies and was somewhat broader than the one we treated. They too encountered convergence difficulties and found that the solution of the EMA equations became more difficult as the resonance was narrowed and moved to lower energies.

[16]L. Schwartz, H. K. Peterson, and A. Bansil, Phys. Rev. B 12, 3113 (1975).

[17]L. Schwartz, Phys. Rev. B 21, 535 (1980).

[18]An equation whose structure is similar to that of (2.2b) is valid in the CPA and can be used to calculate spectral functions and momentum profiles [A. Bansil, R. S. Rao, P. E. Mijnarends, and L. Schwartz, Phys. Rev. B 23, 3608 (1981)].

[19]The six-l symbol

$$\begin{bmatrix} l_1 & l_2 & l_3 \\ l_4 & l_5 & l_6 \end{bmatrix}$$

can be written as

$$\begin{bmatrix} l_1 & l_2 & l_3 \\ l_4 & l_5 & l_6 \end{bmatrix} = \frac{(2l_1+1)(2l_2+1)\cdots(2l_6+1)}{(4\pi)^2} \begin{pmatrix} l_1 & l_2 & l_3 \\ 0 & 0 & 0 \end{pmatrix} \begin{pmatrix} l_1 & l_5 & l_6 \\ 0 & 0 & 0 \end{pmatrix} \begin{pmatrix} l_4 & l_2 & l_6 \\ 0 & 0 & 0 \end{pmatrix} \begin{pmatrix} l_4 & l_5 & l_3 \\ 0 & 0 & 0 \end{pmatrix} \begin{Bmatrix} l_1 & l_2 & l_3 \\ l_4 & l_5 & l_6 \end{Bmatrix} ,$$

where $(\cdots)$ and $\{\cdots\}$ indicate the usual 3-j and 6-j symbols [A. Messiah, *Quantum Mechanics* (North-Holland, Amsterdam, 1969), Appendix C].

[20]P. Lloyd, Proc. Phys. Soc. London 90, 207 (1967); 90, 217 (1967).

[21]L. Schwartz and A. Bansil, Phys. Rev. Lett. 39, 421 (1977); L. Schwartz, Phys. Rev. B 21, 522 (1980).

[22]A. Bansil, H. K. Peterson, and L. Schwartz, Inst. Phys. Conf. Ser. 30, 313 (1976).

[23]This calculation employs the same atomic potential and pair distribution function used in Sec. III. We simply ignore the s and p phase shifts.

[24]See also Fig. 6 of Ref. 9. The $m = 0$ component of $A(k,E)$ is seen to vanish as $k \to \kappa$. For energies above the d resonance, this leads to a spurious minimum near $k = \kappa$.

[25]In Fig. 3(a), the curves were placed on a common energy axis by aligning the upper d-band edges. The ODS was normalized to the EMA curve by requiring the same integrated weight between $E = 0.2$ and $E = 0.7$. The EDC was then normalized by matching its peak height at the upper d-band edge to that of the ODS. In Fig. 3(b), the EDC was normalized by scaling its peak height at the upper d-band edge to that of the EDC shown in (a).

[26]The crystal Cu density of states shown in Fig. 3(b) is also based on the potential described in Ref. 12.

[27]See Fig. 1 of the first paper cited in Ref. 21.